Hindawi
Shock and Vibration
Volume 2021, Article ID 9999007, 18 pages
https://doi.org/10.1155/2021/9999007

Research Article

Effect of Near-Fault Pulsed Ground Motions on Seismic Response and Seismic Performance to Tunnel Structures

Xiancheng Mei,[1,2] **Qian Sheng**,[1,2] **and Zhen Cui**[1,2]

[1]*Institute of Rock and Soil Mechanics, Chinese Academy of Sciences, Wuhan 430071, China*
[2]*University of Chinese Academy of Sciences, Beijing 100049, China*

Correspondence should be addressed to Zhen Cui; zcui@whrsm.ac.cn

Received 25 March 2021; Accepted 29 May 2021; Published 12 June 2021

Academic Editor: Junfei Zhang

Seismic analysis of tunnels close to or crossing seismogenic faults is a complex problem, which is often neglected at the design stage for the lack of specific codes or guidelines and also because underground structures are considered less vulnerable than that of the corresponding above-ground facilities. Near-fault ground motions are generally assumed to providing more powerful energy to tunnel structures. Therefore, a recently developed velocity pulse equivalent model is proposed to synthesize the artificial near-fault pulsed ground motion for the seismic response behavior of the tunnel structure. A newly proposed nonlinear dynamic time history methodology, the incremental dynamic analysis method, is introduced into the analysis of seismic performance and fragility for tunnel structures. This study takes the Zheduoshan tunnel as a case study to illustrate the effects of velocity pulse on the seismic response behavior and seismic performance. The applicability of different seismic intensity measures is preliminarily discussed, and the vulnerability of the tunnel structure at different characteristic locations is analyzed. Afterward, the seismic vulnerability probabilities of the tunnel structure under the action of the near-fault pulsed ground motions and the far-field ground motions are presented, and then, the failure probabilities of the tunnel structure under the three-level support requirements are obtained. Research results provide an objective assessment of the velocity pulse effects and acts as a reference for the likely seismic damage assessment of tunnel structures.

1. Introduction

It is a fact that underground structures are relatively less vulnerable than that of the corresponding above-ground facilities [1, 2]. Since the structural response is constrained by the surrounding rock, the relative deformation of the underground structures such as tunnels and caverns concerning the surrounding rock is usually small [3–5]. Nevertheless, several pieces of literature show that tunnels and underground structures located in the seismically active regions suffered severe damages [6–9]. This phenomenon has attracted widespread attention from scholars at home and abroad. Meanwhile, it is generally difficult for some important transportation tunnels or lifelines for water delivery to avoid crossing seismically active regions or even active faults [10, 11]. Therefore, a special study on the effect of near-fault ground motions on the tunnel structures is required.

The near-fault ground motion generally refers to the ground motion where the engineering site is not more than 20 km away from the seismogenic fault [12, 13]. Because of the focal mechanism and the attenuation characteristics of seismic waves, the most significant difference between near-fault ground motions and far-field ground motions is the velocity pulse waveform generated by the directional effect and the sliding effect. The velocity pulse has the characteristics of a simple waveform, strong action, and long period. Shimizu et al. [14] discovered that the tunnel has the greatest damage with magnitude 7 and epicenter distance of 10 km or magnitude 8 and epicenter distance of 20 km all belong to the category of near-fault ground motions, based on the statistical review of the previous major earthquakes in Japan. Housner and Hudson [15] observed that near-fault ground motions are still very destructive even when the magnitude and PGA both are small. [16, 17] analyzed the stability of the underground caverns of Baihetan

hydropower station under the action of near-fault ground motions by using synthetic near-fault pulsed ground motions as the incident ground motion. Song and Gao [18] selected a large number of near-fault pulsed ground motion from the Pacific Earthquake Engineering Research Center Database (PEER) and analyzed the correlation between the slope seismic displacement and the parameters of velocity-pulsed ground motions through numerical calculation. The above literature review reveals that the impact and harm of near-fault ground motions on the seismic dynamic response of underground engineering have been researched. There are some works about the velocity pulse effect of near-fault ground motions [19–21]. However, the impact of the velocity pulse effect of near-fault ground motions on the seismic performance of tunnel engineering is still not clear.

The performance-based earthquake engineering (PBEE) is a seismic design theory in the spotlight in the engineering aseismic discipline, and it is regarded as the main guiding ideology of seismic design [22, 23]. Incremental dynamic analysis (IDA) is a newly proposed PBEE analysis method based on nonlinear dynamic time history analysis [24–26]. The ground motion parameters are adjusted and amplified step by step through the intensity measure (IM) of the ground motion to become a group of ground motions with multiple intensities, and then, the nonlinear dynamic time history analysis is performed under the action of these ground motions to obtain sufficient damage measure (DM) of engineering structures and the corresponding IM values. Thus, an IDA curve that can characterize the whole process of engineering structure from an elastic state to a plastic state to complete failure state under a certain ground motion is obtained. Based on IDA curve clusters, regression fitting analysis and data statistics methods can be employed to conduct seismic vulnerability analysis, and finally, the limit state of the structure at different performance levels and the failure probability of each performance level are discovered. Cui [27] introduced the IDA method into the field of performance optimization and seismic dynamic stability evaluation of large-scale underground cavern groups, providing criteria for the research of seismic dynamic catastrophic instability of it. Zhong [28] introduced the IDA method into the seismic vulnerability analysis of subway station structures and established a seismic vulnerability curve for shallow-buried subway station structures, which quantified the failure probability of the structure under different performance levels.

The present study considers the Zheduoshan tunnel as the case study, aiming at analyzing the influence of the near-fault pulsed ground motion on the seismic response of the tunnel structure and introducing the IDA approach for the seismic performance to compare the seismic vulnerability probability of tunnel structure under the action of near-fault pulsed ground motion and far-field ground motion. Additionally, the near-fault pulsed ground motion and far-field ground motion synthesized by the velocity pulse equivalent model are employed. The vulnerable area and the failure probability of the tunnel structure are evaluated and quantified. This study provides an objective assessment of the velocity pulse effects and acts as a reference for the likely seismic damage assessment of tunnel structures.

2. Zheduoshan Tunnel of Sichuan-Tibet Railway

2.1. Characteristics of the Tunnel. The Zheduoshan tunnel is a key control part of the Sichuan-Tibet railway line, a national strategic project, which is the second railway to reach the Tibet Plateau in China. This is a 20.89 km long tunnel with a maximum cover of 1235 m. This tunnel is chosen as a case study due to the crossing of many faults and the relevant seismicity of the region, as shown in Figure 1. The tunnel traverses several major faults such as Zheduotang fault, Jinglong temple-Mozigou fault, Huiyuan temple-Legip fault, and Yulongxi fault, all with a width of several tens of meters. Meanwhile, the South-North seismic belt, where the Zheduoshan tunnel is located, is one of the most active seismic territories in China. This region has been struck by several large destructive earthquakes that occurred in Kangding 1786 and 2014 ($M_s = 7.5$, 6.3), Ya'an 2013 ($M_s = 7.0$), and Mao county 1933 ($M_s = 7.5$), as shown in Figure 1(a). According to the seismic ground motion parameter zonation map of China (2015), the basis seismic intensity of the Zheduoshan tunnel site area is VIII degree and the characteristic period of the ground motion response spectrum is 0.4 s. Due to the above characteristics, the Zheduoshan tunnel is seriously threatened by near-fault earthquakes.

2.2. Setup of the Numerical Model. Based on the Zheduoshan tunnel with a four-centered arched section, the numerical model is established by the finite different method FLAC 3D 6.0 in this manuscript, as shown in Figure 2. The maximum height of the vault-arch bottom is 10.15 m, while the maximum width of the sidewalls on both sides is 11.42 m and the lining thickness is 0.7 m. The maximum grid size is 5 m, which needs to meet the requirement $\Delta l \leq \lambda/10$ for the input ground motion fidelity [29–31]. Based on the following equations (1)–(3) and the parameters in Table 1, the maximum frequency which can be accurately modeled by the model is 16.36 Hz. The Mohr–Coulomb yield criterion is set for the model, so that the elastoplastic dynamic time history analyses are more representative. In this study, the constitutive model of the surrounding rock solid elements is set by the strain-hardening model to simulate type IV rock, while the Mohr–Coulomb model is to simulate C30 concrete for the lining solid elements. In additional, the tunnel-ground interaction relationship is neglected, so that there are no tunnel-ground interfaces in the model. The physical and mechanical parameters used in the numerical simulation are given in Table 1 [32, 33].

$$G_s = \frac{E}{2}(1 + \nu), \tag{1}$$

$$C_s = \sqrt{\frac{G_s}{\rho}}, \tag{2}$$

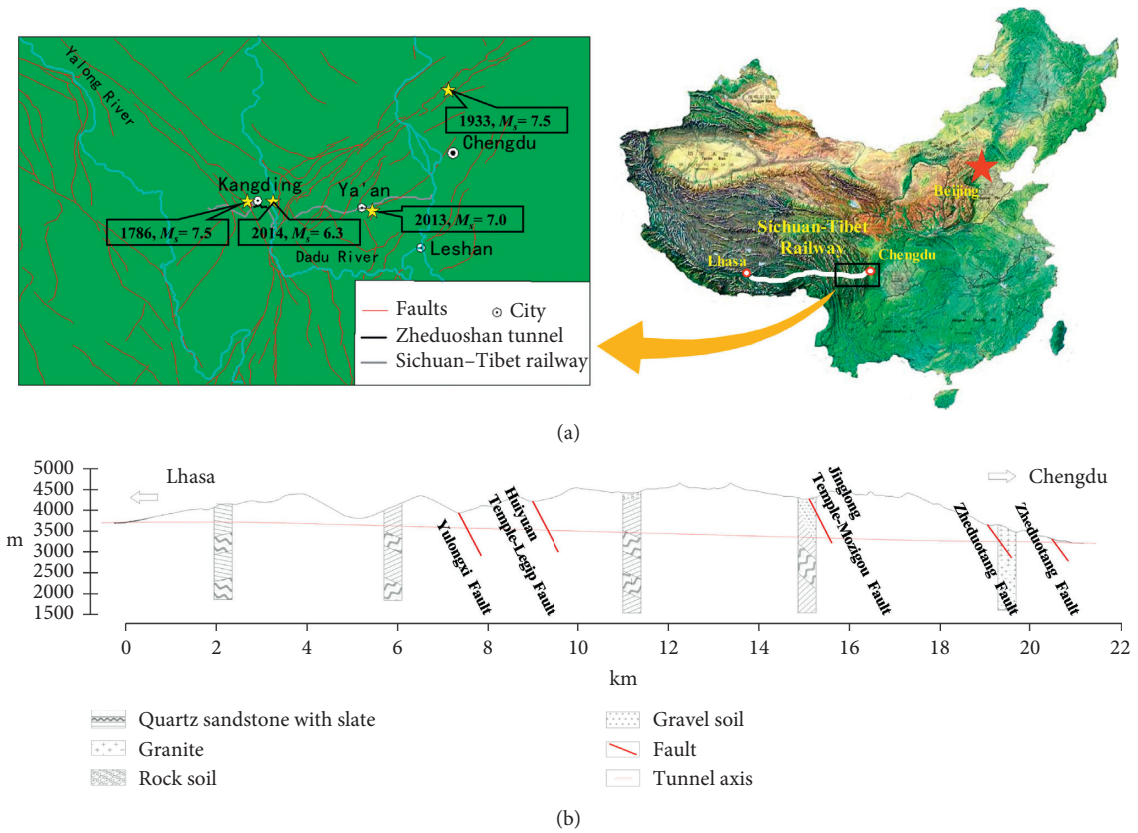

Figure 1: (a) Location of the Zheduoshan tunnel along the Sichuan-Tibet railway line and the earthquake events. (b) Geological profile along the Zheduoshan tunnel.

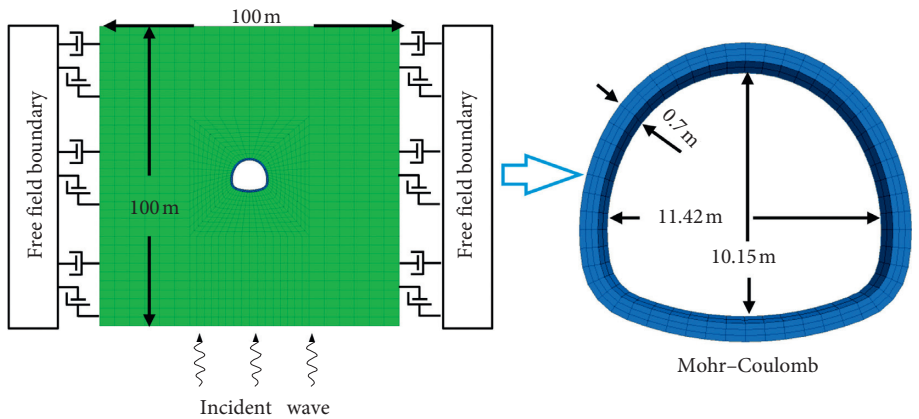

Figure 2: Calculation model of Zheduoshan tunnel.

Table 1: Physical and mechanical parameters used in the numerical simulation.

Group	E (GPa)	ν	ρ (kg·m^{-3})	c (MPa)	$\varnothing$ (°)	f_t (MPa)
Rock mass	4.0	0.3	2300	0.5	33.0	4.0
Lining	30	0.3	2300	3.18	54.9	1.23

$$f = \frac{C_s}{\lambda} = \frac{C_s}{10\Delta l}, \tag{3}$$

where G_s is the shear modulus of the field, C_s is the wave velocity in the field, f is the frequency of input motions, λ is the wavelength corresponding to the maximum frequency, and Δl is the maximum grid size.

To reduce the reflection of seismic waves from the model boundary, free-field artificial boundaries are set on both sides of the model to replace the previous displacement constraints, after the static calculation is completed and the model reaches equilibrium [34–36]. Meanwhile, the incident wave is input from the bottom boundary of the model with the stress time history curve, which is converted from the seismic velocity time history curve. The combined local damping model is adopted for representing the mechanical damping behavior. This manuscript does not consider the effect of the tunnel-rock interaction on the seismic response of the lining.

3. Seismic Response of the Tunnel Subjected to Synthetic Ground Motions

To compare the difference in the seismic response of the tunnel structure under the excitation of the near-fault velocity-pulsed ground motion and the far-field motion, these two different ground motions were artificially synthesized, according to the seismic and geological parameters of the Zheduoshan tunnel site region. Afterward, the seismic response analysis of the tunnel structure is carried out in terms of the deformation, the principal stress, and the plastic failure distribution.

3.1. Synthetic of Artificial Ground Motions

3.1.1. Artificial Far-Field Ground Motion. According to the Chinese code for seismic design of railway engineering (2006), the site design response spectrum is presented in the form of dynamic amplification factor β, as shown in Figure 3(a). The response spectrum expression is

$$\beta = \begin{cases} 1 + 12.5T, & 0 < T < 0.1, \\ 2.25, & 0.1 < T < T_g, \\ 2.25\left(\dfrac{T_g}{T}\right), & T_g < T < 5T_g, \\ 0.45, & 5T_g < T < 2, \end{cases} \tag{4}$$

where β is the dynamic amplification factor, T is the seismic period, and T_g is the characteristic period of the response spectrum.

Then, the artificial far-field ground motion is synthesized using the SeismoArtif software, based on the site design response spectrum. Figure 3(c) shows the acceleration, velocity, and displacement time history of the far-field ground motion.

3.1.2. Artificial Near-Fault Velocity Pulsed Ground Motion. The input ground motion can be approximated by considering the only double-pulse ground motion when analyzing the impact of near-fault ground motions on structure damage [37]. The equivalent velocity pulsed model in terms of V_p, T_p, and ratio is utilized in this manuscript [37]. Based on the equivalent velocity pulsed model, the expression of the equivalent model is

$$v(t) = \begin{cases} V_p \sin\left(\omega_p (t - t_0)\right), & t_0 < t < t_0 + \dfrac{T_p}{2}, \\ \text{Ratio} \cdot V_p \sin\left(\omega_p (t - t_0)\right), & t_0 + \dfrac{T_p}{2} < t < t_0 + T_p, \end{cases} \tag{5}$$

$$V_p = \max\left(\left|V_{p1}\right|, \left|V_{p2}\right|\right), \tag{6}$$

$$\text{Ratio} = \min\left(\left|\frac{V_{p1}}{V_p}\right|, \left|\frac{V_{p2}}{V_p}\right|\right), \tag{7}$$

where V_p is the peak pulse velocity, T_p is the pulse period, t_0 is the start time of velocity pulse, V_{p1} and V_{p2} are the positive velocity peak and negative velocity peak of the ground motion, respectively, and ratio is the larger value of the ratio of the positive velocity peak and the negative velocity peak to the pulse velocity peak.

For the V_p, T_p, and ratio, the attenuation formula of the equivalent pulsed model is

$$\ln T_p = a_1 + a_2 M_w, \tag{8}$$

$$\ln V_p = b_1 M_w + b_2 d_r + b_3, \tag{9}$$

$$\ln \text{ratio} = c_1 M_w + c_2 d_r + c_3, \tag{10}$$

where a_1, a_2, b_1, b_2, b_3, c_1, c_2, and c_3 are the regression coefficients related to a seismogenic fault, which are determined according to Table 2, and the M_w is the moment magnitude.

This study optimizes the filtering range based on the existing methods [38, 39]. That is, the high-frequency components of the velocity time history which are greater than $(1/T_p)$ Hz are obtained by limiting the Fourier spectrum bandwidth in the synthesis process, and the components less than $(1/T_p)$ Hz are obtained by derivation of the equivalent velocity pulsed model. The specific synthesis process of the ground motion is

(1) For the velocity pulse components of frequency less than $(1/T_p)$ Hz, the V_p, T_p, and ratio are determined by equations (8)–(10), according to the seismic geological parameters of the specific site. So, the velocity pulse time history is generated, and then, the acceleration time history is obtained by derivation calculus to the velocity pulse time history.

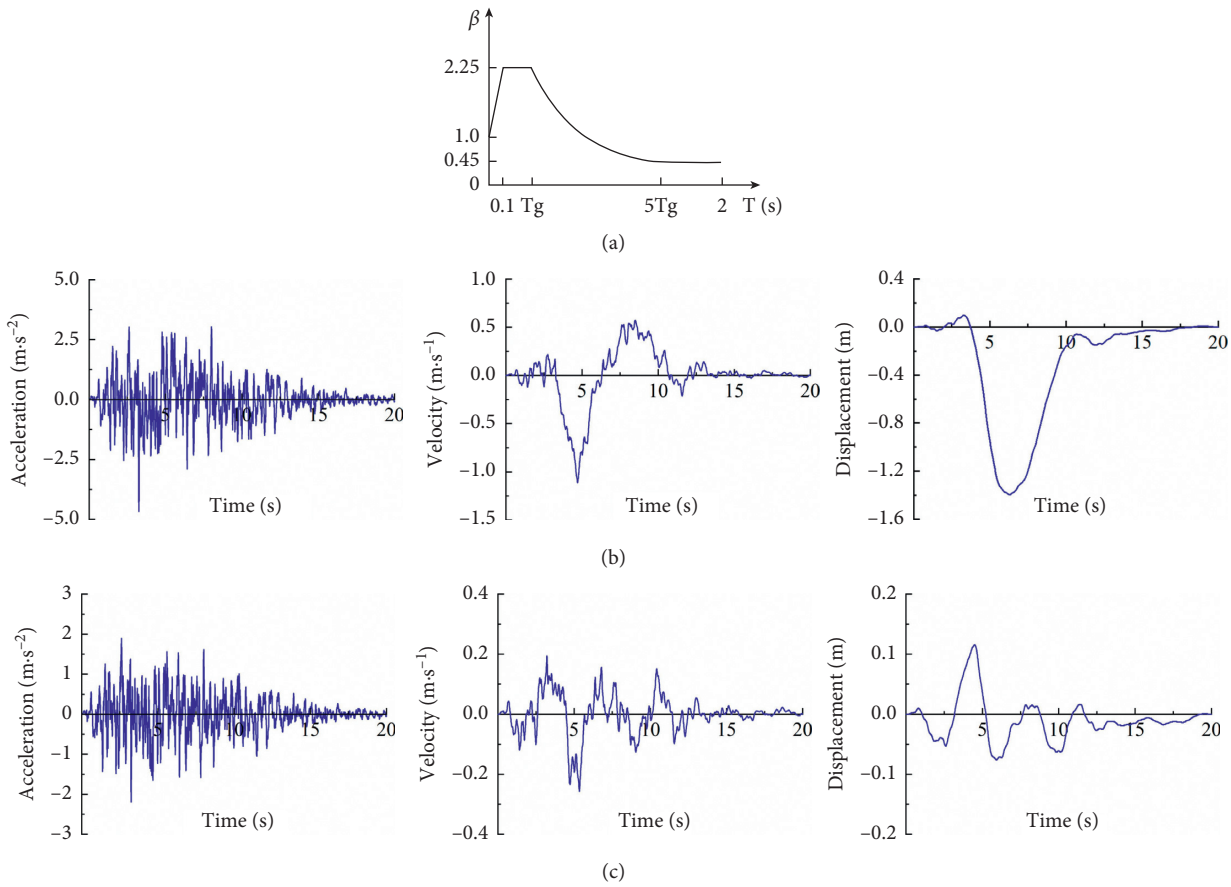

Figure 3: (a) The Zheduoshan tunnel site design response spectrum. (b) The time history curves of near-fault pulsed ground motion. (c) The time history curves of far-field ground motion.

Table 2: The regression coefficients and the variance of T_p, V_p, and ratio for different faults.

Type	T_p			V_p				Ratio			
	a_1	a_2	σ_1	b_1	b_2	b_3	σ_2	c_1	c_2	c_3	σ_3
All	−5.3	0.92	0.11	0.40	−0.05	1.81	0.64	0.1344	−0.0054	−1.2328	0.2245
Reverse fault and mixed fault	−9.2	1.41	0.34	0.10	−0.09	5.07	0.63	0.0007	−0.0004	−0.4303	0.1773
Strike-slip fault	−5.9	1.04	0.08	0.52	-0.05	0.90	0.59	0.4376	−0.0048	−3.1306	0.2507

(2) For the high-frequency components of acceleration, according to the seismic geological parameters of the specific site, the artificial ground motion is synthesized with the requirement that the Fourier spectrum bandwidth is above $(1/T_p)$ Hz.

(3) Translate the low- and high-frequency components generated by the above method, according to certain assumptions. And then, the high-frequency components are amplitude-modulated, so that the total amplitude after the addition of high- and low-frequency components is equal to the amplitude of the ground motion propagating to the site according to the attenuation relationship when the seismogenic fault induces a certain magnitude earthquake.

Regarding the Zheduotang fault as the seismogenic fault, the upper limit of the moment magnitude is 7.5. When an upper limit earthquake occurs at the potential source, the acceleration amplitude propagated to the site of Zheduoshan tunnel is 467 gal, considering the attenuation relationship of ground motion propagation. The Zheduotang fault is about 30 km long and is a left-lateral strike-slip fault. According to the regression values of the corresponding parameters given in Table 2 and combined with equations (5)–(10), the V_p, T_p, and ratio are, respectively, equal to 73.70 cm/s, 6.69 s, and 0.82. Afterward, the time history curves of the near-fault pulsed ground motion are synthesized using the above-mentioned synthesis method, as shown in Figure 3(b).

3.2. Comparison of Seismic Response of the Tunnel Structure Subjected to Synthetic Ground Motions. Based on the artificially synthesized near-fault pulse ground motions and far-field ground motions under the same geological seismic

conditions, the relative deformation rate, maximum principal stress of the structure, and the overall plastic failure of the model are obtained with these different ground motions excitation.

3.2.1. Relative Deformation Rate. Figure 4(a) shows the time history records of relative deformation rate between vault and arch bottom of tunnel structure under the near-fault pulsed and far-field ground motions excitation. It can be seen that under the action of the near-fault pulsed ground motion, the relative deformation rate of the vault-arch bottom of the tunnel structure reaches its peak at around 5^{th} second when the velocity pulse arrives, then it drops back, and finally maintains a permanent displacement of 31.27 mm. However, eventhough the peaks of the relative deformation rate are almost equal in both different cases, it remains fluctuating with the far-field ground motion, and only a permanent deformation of 0.28 mm remains at the end, as shown in Figure 4(c).

Figure 4(b) illustrates the time history records of relative deformation rate between the sidewalls between both sides of the tunnel structure under the near-fault pulsed and far-field ground motions excitation. The trend is similar to the relative deformation rate between the vault and arch bottom under the action of these two kinds of ground motions. At the same time, under the action of the near-fault pulsed ground motion, the permanent relative deformation of the sidewalls between both sides is 29.04 mm, while it is only 0.31 mm under the action of the far-field ground motion.

3.2.2. Principal Stress and Plastic Failure. As shown in Figure 5(a), when the model is under the action of the near-fault pulsed ground motion, the maximum principal stress peak at each characteristic location of the tunnel structure increases, especially it increases significantly at the vault and sidewalls on both sides. With the excitation of the near-fault pulsed ground motion, it was discovered that the plastic zone volume of the rock mass only increased by a small amount before the arrival of the velocity pulse, and it increased suddenly and sharply during 4 s to 5 s. There was a small increase during the period from 5 s to 9 s and then reached the maximum after 9 s, as shown in Figure 5(b). The time when the volume of the plastic zone begins to increase sharply is the same as the arrival time of the velocity pulse. Meanwhile, the period from 4 s to 9 s is almost equal to the arrival time of the velocity pulse, indicating that the velocity pulse provides the major energy in the excitation of near-fault pulsed ground motion.

Summarily, the near-fault pulsed ground motion is more destructive to tunnel structure than far-field ground motion, that is, because the velocity pulse plays a significant role in the action of near-fault pulsed ground motions and is an influential factor that cannot be ignored.

4. Seismic Performance of Tunnel Structure Based on the IDA Method

4.1. Analysis Process of IDA. As shown in Figure 6, the specific analysis process of IDA is

(1) Establish a suitable elastoplastic analysis model for the engineering background

(2) Select a series of ground motions that can reflect the ground motion engineering characteristics, based on the site design response spectrum of the engineering region

(3) Determine the appropriate seismic intensity measure (IM) and structural damage measure (DM), according to the engineering characteristics of the engineering

(4) Draw a set of curve cluster with the IM as the ordinate against the DM as the abscissa, based on numerous dynamic time history calculation analysis results. These calculation results are determined by the multiple sets of ground motion input parameters including a wide range of intensities, which are obtained by stepwise amplification.

(5) Draw the seismic vulnerability curve of the structure by the regression fitting analysis and data statistics methods, and then, the failure probability of the structure under different performance levels is obtained.

This study has established the Zheduoshan tunnel model in Section 2.2, which is available for the seismic performance analysis of the tunnel structure with IDA. Afterward, according to the above IDA process, the vulnerability of the tunnel structure at different characteristic locations are analyzed, and the seismic vulnerability of the structure under the excitation of near-fault pulsed ground motions and far-field ground motions are further comparative analyzed.

4.1.1. Selection of Ground Motion Records Based on PEER Database. The ground motion induced by the seismic wave is strongly random in the propagation process. Furthermore, the different characteristics of the ground motion have a great influence on the analysis results of the tunnel seismic response and failure mechanism. However, 10–20 ground motion records utilized in IDA are sufficient to eradicate the uncertain effects of ground motion [25, 26]. In this study, based on the site design response spectrum, epicenter distance, intensity, and whether to consider velocity pulse as indicators, a total of 24 records of near-fault pulsed ground motion and far-field ground motion are selected from the Pacific Earthquake Engineering Research Center Database (PEER) by the selection system of the Design Ground Motion Library (DGML). Table 3 presents the specific information of the selected ground motion records. The moment magnitude of selected records is within the range of 3.5–8. Additionally, 12 near-fault pulsed ground motions with an epicenter distance of 0–20 km and 12 far-field ground motions with an epicenter distance of 20–100 km were determined by the DGML. Figure 7(a) shows the distribution relationship between the PGA of the selected ground motions and the epicenter distance, which indicates the selected ground motions can reflect the randomness of ground motion. Meanwhile, from the comparison of the

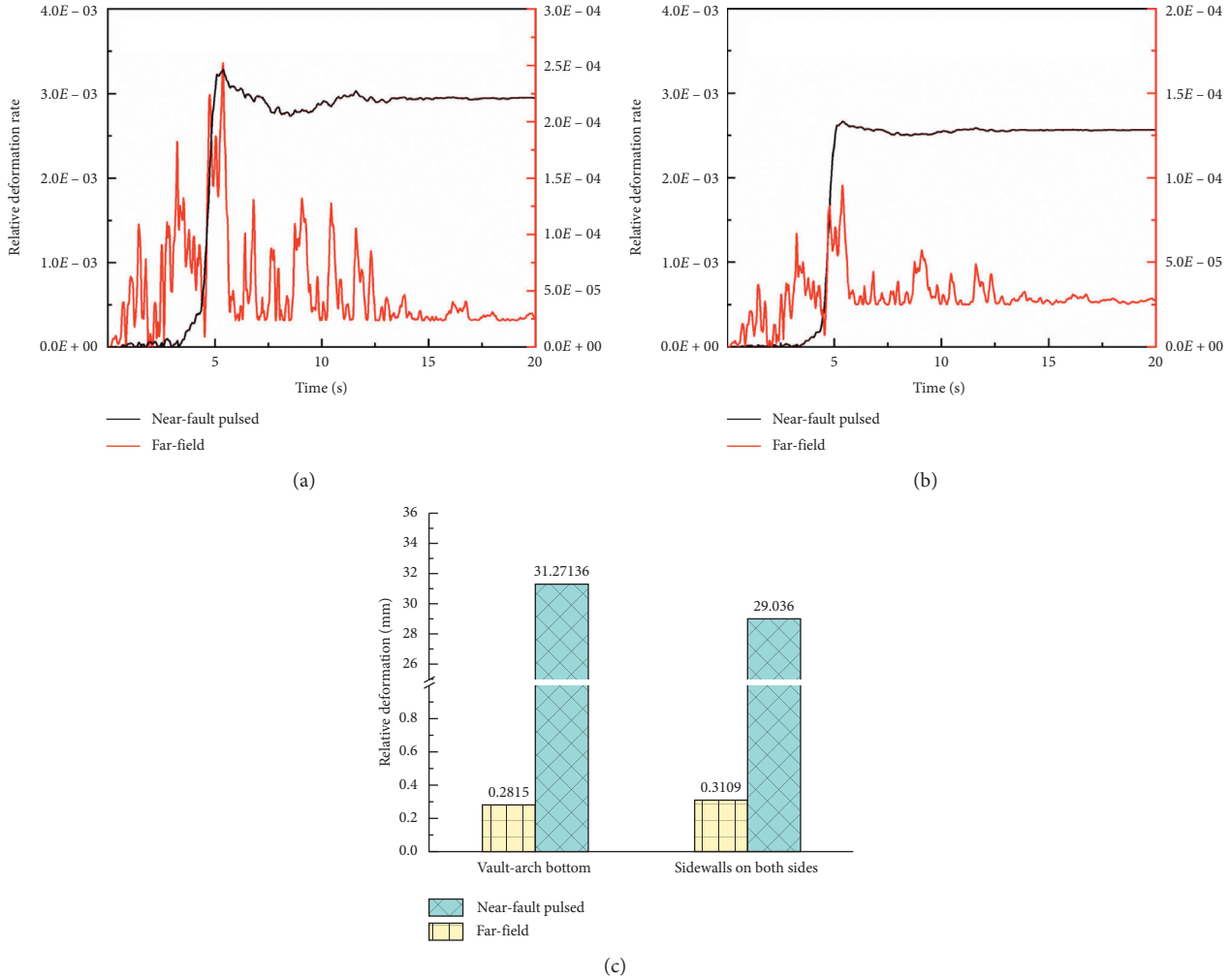

Figure 4: Relative deformation of the tunnel structure under different action of ground motions. (a) The relative deformation rate of the vault-arch bottom of the tunnel structure. (b) The relative deformation rate of the sidewalls on both sides of the tunnel structure. (c) The comparison of the relative deformation of the vault-arch bottom and the sidewalls on both sides.

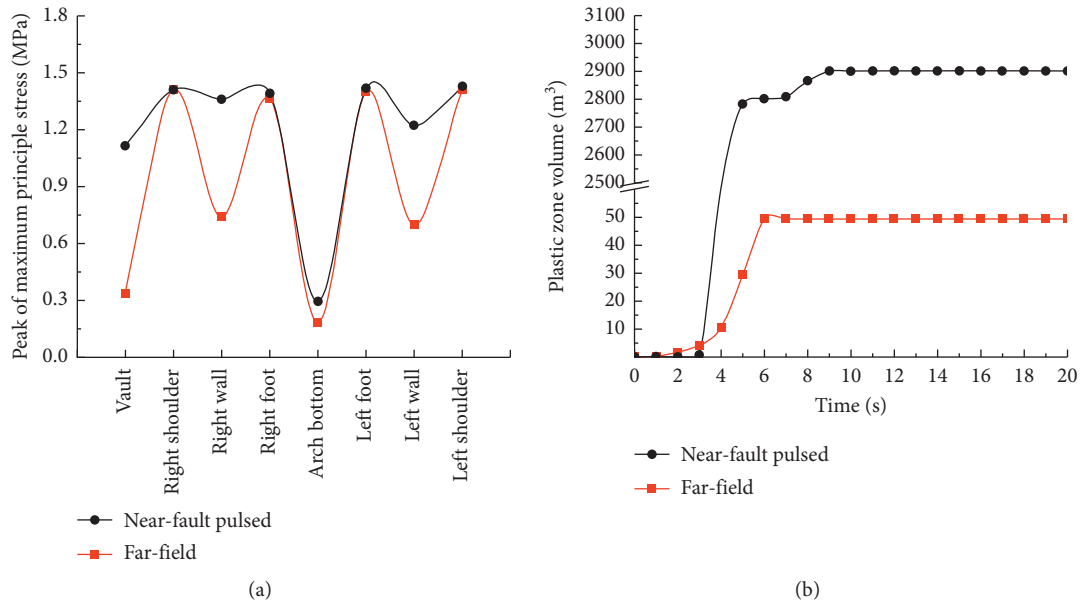

Figure 5: The comparison of the principal stress of the structure and the plastic failure zone of the model under different ground motions. (a) The principal stress of the tunnel structure. (b) The plastic failure zone volume of the tunnel model.

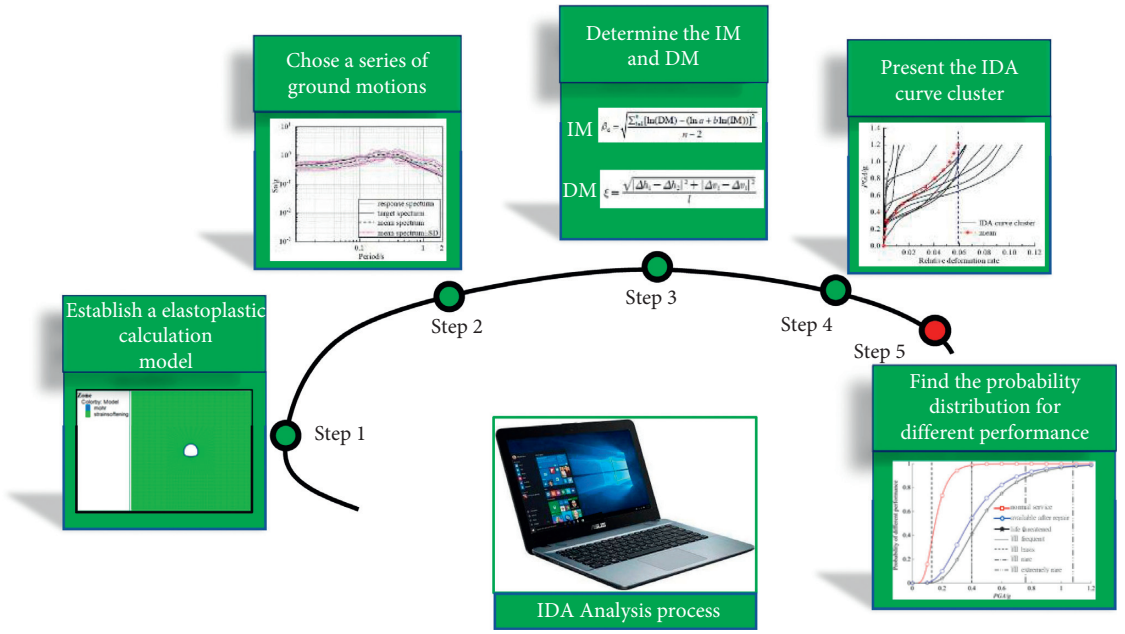

Figure 6: The specific analysis process of IDA.

Table 3: The specific information about the selected ground motion records.

Type	ID	Station	Year	PGA (g)	PGV (m/s)	PGD (m)	Magnitude (M_w)	Effective duration (s)	T_p (s)	Epicenter distance (km)	Earthquake name
Near-fault pulsed ground motion	1	RSN161-Brawley Airport	1979	0.152	0.087	0.037	6.53	11.13	4.40	10.42	Imperial Valley-06
	2	RSN178-El Centro Array #3	1979	0.127	0.044	0.047	6.53	22.08	4.50	12.85	Imperial Valley-06
	3	RSN179-El Centro array #4	1979	0.269	0.167	0.115	6.53	19.43	4.79	7.05	Imperial Valley-06
	4	RSN185-Holtville Post Office	1979	0.257	0.057	0.190	6.53	9.58	4.82	7.5	Imperial Valley-06
	5	RSN292-Sturno (STN)	1980	0.225	0.199	0.071	6.9	12.108	3.27	10.84	Irpinia-Italy-01
	6	RSN764-Gilroy-Historic Bldg.	1989	0.148	0.125	0.081	6.93	11.24	1.64	10.97	Loma Prieta
	7	RSN766-Gilroy Array #2	1989	0.295	0.083	0.024	6.93	9.00	1.73	11.07	Loma Prieta
	8	RSN1050-Pacoima Dam (downstr)	1994	0.191	0.074	0.030	6.69	7.28	0.59	7.01	Northridge-01
	9	RSN1052-Pacoima Kagel Canyon	1994	0.169	0.074	0.021	6.69	11.50	0.73	7.26	Northridge-01
	10	RSN1165-Izmit	1999	0.144	0.061	0.029	7.51	16.74	5.37	7.21	Kocaeli Turkey
	11	RSN3746-Centerville Beach_ Naval Fac	1992	0.121	0.085	0.022	7.01	14.22	1.97	18.31	Cape Mendocino
	12	RSN4458-Ulcinj-Hotel Olimpic	1979	0.423	0.073	0.029	7.1	9.88	1.97	5.76	Montenegro Yugoslavia

Table 3: Continued.

Type	ID	Station	Year	PGA (g)	PGV (m/s)	PGD (m)	Magnitude (M_w)	Effective duration (s)	T_p (s)	Epicenter distance (km)	Earthquake name
Far-field ground motion	1	RSN-787-Palo Alto-SLAC Lab	1989	0.089	0.107	0.160	6.93	17.48	/	30.86	Loma Prieta
	2	RSN-990-LA-City Terrace	1994	0.135	0.072	0.018	6.69	15.72	/	36.62	Northridge-01
	3	RSN-4455-Herceg Novi-O.S.D. Paviviv	1979	0.210	0.050	0.127	7.1	12.00	/	25.55	Montenegro_Yugoslavia
	4	RSN-4841-Joetsu Yasuzukaku Yasuzuka	2007	0.050	0.057	0.038	6.8	24.86	/	25.52	Chuetsu-Oki_Japan
	5	RSN-4846-Joetsu Yanagishima paddocks	2007	0.175	0.120	0.039	6.8	10.98	/	31.43	Chuetsu-Oki_Japan
	6	RSN-4852-Joetsu_Aramaki district	2007	0.064	0.059	0.034	6.8	25.58	/	32.54	Chuetsu-Oki_Japan
	7	RSN-4858-Tokamachi, Chitosecho	2007	0.069	0.094	0.056	6.8	29.76	/	30.65	Chuetsu-Oki_Japan
	8	RSN-4869-Kawaguchi	2007	0.071	0.082	0.035	6.8	27.34	/	29.25	Chuetsu-Oki_Japan
	9	RSN-5775-Tamati Ono	2008	0.138	0.081	0.037	6.9	19.08	/	28.91	Iwate_Japan
	10	RSN-5778-Matsuyama city	2008	0.084	0.060	0.038	6.9	24.08	/	40.98	Iwate_Japan
	11	RSN-5804-Yamauchi Tsuchibuchi, Yokote	2008	0.170	0.049	0.019	6.9	12.74	/	28.41	Iwate_Japan
	12	RSN-5806-Yuzawa town	2008	0.117	0.155	0.042	6.9	17.26	/	25.56	Iwate_Japan

acceleration response spectrum of the selected ground motions with the design response target spectrum of Zheduoshan site as shown in Figures 7(b) and 7(c), it can be seen that the response spectrum of selected ground motions is fit for the site design target spectrum, which indicates that the selected ground motions can reflect the site ground motion characteristics of Zheduoshan tunnel.

According to the probability of an earthquake [40], ground motions are divided into frequent ground motions with a 50-year exceeding probability of 63%, basis ground motions with a 50-year exceeding probability of 10%, rare ground motions with a 50-year exceeding probability of 2%, and extremely rare ground motions with a 100-year exceeding probability of 1%, and their determination coefficients of corresponding ground motion parameters are stipulated. Under the condition that the basic support intensity of the engineering site is VIII degree and the *PGA* of the basic ground motion is 0.4 g, the *PGA* of other intensity ground motions are determined as given in Table 4. Therefore, considering the extremely rare ground motion, 24 ground motions are adjusted according to 0.1 g, 0.2 g–1.2 g using the *PGA* as the basis for amplitude modulation. And then, a total of 288 calculation schemes are obtained.

4.1.2. Selection of DM and IM. The DM is an index representing the seismic performance of the structure in the IDA curve. There are many indicators for evaluating the seismic performance of concrete structures, such as displacement, strain, and cumulative damage [28, 41]. Underground structures such as tunnels only need to be able to keep the line space unobstructed in terms of function. Therefore, many scholars have selected the interstory displacement angle and diameter deformation rate as indicators of rectangular and circular tunnel structural damage, respectively, while there are few indicators for the four-centered arched tunnel. In this study, the relative deformation rate of the line between the left foot and the right shoulder of the tunnel is selected as DM to characterize the structural damage of the four-centered arched tunnel [42].

$$\xi = \frac{\sqrt{\left|\Delta h_1 - \Delta h_2\right|^2 + \left|\Delta v_1 - \Delta v_2\right|^2}}{l}, \tag{11}$$

where ξ is the relative deformation rate; Δh_1 and Δh_2 are the horizontal and vertical displacements of the left foot, respectively; Δv_1 and Δv_2 are the horizontal and vertical displacements of the right shoulder, respectively; and the l is

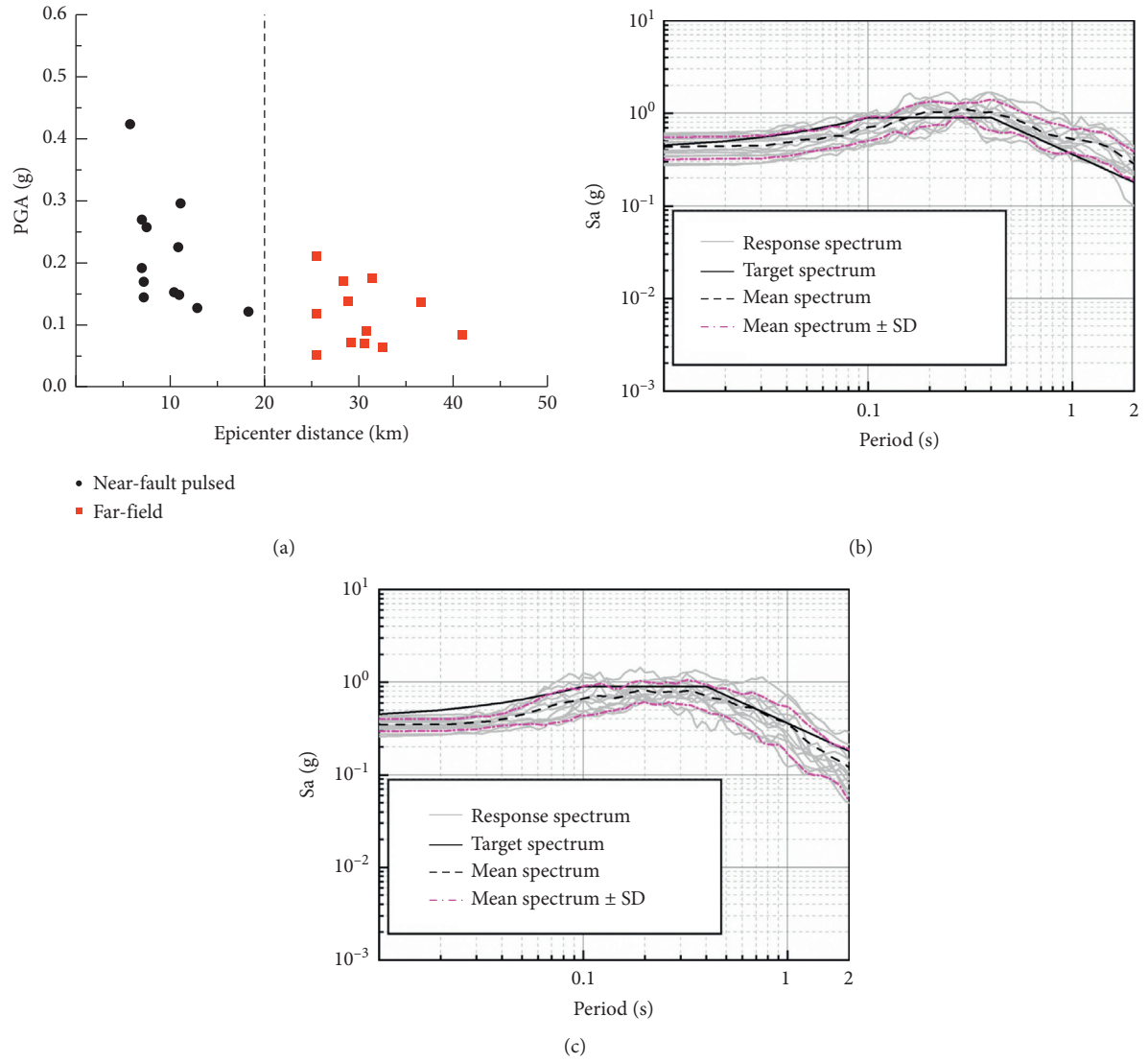

Figure 7: The ground motions selected from the PEER. (a) The distribution relationship between PGA and the epicentral distance of selected seismic. (b) The response spectrum of near-fault pulsed ground motions. (c) The response spectrum of far-field ground motions.

Table 4: Calculation scheme of controlling variable method of different interface parameters.

Fortification intensity	Frequent ground motion	Basis ground motion	Rare ground motion	Extremely rare ground motion
VIII degree	0.13 g	0.4 g	0.746 g	1.08 g
Exceeding probability	50-year 63%	50-year 10%	50-year 2%	100-year 1%

the linear distance between the left foot and the right shoulder.

The IM is an index representing the intensity of the ground motion in the IDA curve, such as *PGA*, *PGV*, *PGD,* and S_a (T_1, 5%) [43]. To select an IM that can comprehensively and efficiently reflect the elastoplastic seismic time history analysis of the tunnel structure, the most appropriate IM is determined by comparing the dispersion of IDA results under these different IM. There has not been a mature conclusion about the natural vibration period of the underground tunnel engineering which is a cavern located in a semiinfinite space. Therefore, in this study, only the *PGA*, *PGV,* and *PGD* are considered as IM that affects the dispersion of IDA results. By linear regression of DM of the IDA results and the logarithmic value of the corresponding IM, the regression coefficients a and b corresponding to different IM are, respectively, fitted to obtain the linear relationship shown in formula (12). Then, the average

standard deviation S of the linear fitting is found according to formula (13).

$$y = ax + b, \tag{12}$$

$$S = \sqrt{\frac{\sum_{i=1}^{n} [\ln(\mathrm{DM}) - (a \ln(\mathrm{DM}) + b)]^2}{n-1}}, \tag{13}$$

where x and y are the different IM values and the logarithm of their corresponding DM, respectively; a and b are linear fitting coefficients; S is the average standard deviation of the IDA results corresponding to different IM indicators; n is the number of calculation for nonlinear dynamic time history analysis, and the value is 144.

By comparing the regression fitting of different IM indicators and their corresponding average standard deviations (as shown in Figure 8), it can be found that the S of *PGA* as the indicator is smaller than *PGV* and *PGD*. The smaller the S, the more suitable the corresponding parameter is as an IM indicator. Meanwhile, PGA is utilized as an indicator of ground motion amplitude in various codes, and the earthquake risk analysis results of various engineering are presented in the form of PGA. Summarily, PGA selected as the IM in this study is the most suitable.

4.1.3. Classification of Seismic Performance Level. The classification result of the seismic performance level will directly affect the trend of the seismic vulnerability curve. Thus, to obtain the correct seismic vulnerability curve, it is necessary to determine the threshold of structural damage state under different performance levels. According to the code for seismic design of railway engineering [44], the seismic design of railway engineering should meet the seismic performance requirements given in Table 5, and the support targets under the corresponding support requirements are defined. The seismic performance level of the tunnel structure is a limit failure state, which refers to the maximum damage degree of the structure under the support requirement. Meanwhile, the study [42] verified the bearing capacity and the deformation of the tunnel structure under different support requirements, and combined with the research results of the seismic index of the rectangular section and the circular section tunnel, the control indexes of the arch tunnel structure damage under various performance requirements are selected, and the thresholds of performance level under the three-level support requirements are determined, as given in Table 5.

Therefore, this study divides the seismic damage state of the railway tunnel structure into four levels: intact, slightly damaged, moderately damaged, and severely damaged, and the classification standard for the seismic damage level of the tunnel structure in terms of the relative deformation rate is established. That is, when $\xi \le \xi_1$, the tunnel structure is in an intact state, when $\xi_1 \le \xi \le \xi_2$, the tunnel is in a slightly damaged state, when $\xi_2 \le \xi \le \xi_3$, the tunnel is in a moderately damaged state, and when $\xi \ge \xi_3$, the tunnel is in a severely damaged state, as given in Table 6.

4.2. Analysis on Seismic Performance of the Tunnel Structure

4.2.1. Vulnerable Area. To analyze the vulnerable area of different characteristic locations of the tunnel section, the IM-horizontal relative deformation rate relationship curve of each location is established from the calculation results. It is found that the calculation results of 24 ground motions have a similar trend. This study only compares the near-fault pulsed ground motion RSN764 with a duration of 39.99 s and a far-field ground motion RSN-990 with a duration of 40.00 s, as shown in Figure 9.

Under the action of these two ground motions, the horizontal relative deformation of the tunnel structure is symmetrically distributed along the central axis of the tunnel section. Afterward, the deformation of the tunnel structure at the sidewalls on both sides is the most serious, which is the vulnerable area of the tunnel. And the second is the shoulders and foot on both sides. The least serious is the vault and arch bottom, and there is almost no deformation in the horizontal direction. Comparing these curves under these different kinds of ground motions, it can be discovered that with the PGA changing, the tunnel structure under the action of the near-fault ground motion is more severely damaged than that of the far-field ground motion under the condition of the same PGA. This indicates that the near-fault pulsed ground motion is more destructive to the tunnel structure than the far-field ground motion.

4.2.2. Seismic Fragility. Figure 10 shows the IM-DM relationship under the action of near-fault pulsed ground motions and far-field ground motions which are IDA curve clusters. It can be observed from the IDA curve clusters that the curves are dense in the initial stage. Afterward, with the earthquake intensity increases, the dispersion of the results gradually increases, indicating that the seismic response of the tunnel structure is closely related to the incident ground motion characteristics. By comparing the IDA curve clusters under the action of near-fault pulsed ground motions and far-field ground motions, it can be found that (1) under the action of the near-fault pulsed ground motions, when the PGA<0.1 g~0.2 g, the relative deformation of the tunnel structure is almost equal to zero because the structure is in an elastic state without damage. Under the action of far-field ground motions, when PGA<0.2 g~0.3 g, the relative deformation of the tunnel structure is almost equal to zero. It can be concluded that compared with far-field ground motions, near-fault ground motions can cause damage to the tunnel structure at relatively slight ground motion intensity. (2) From the average curve, as shown in Figure 10, when PGA reaches 1.2 g, the mean DM under the action of near-fault pulsed ground motions is 0.083, while the mean DM under the action of far-field ground motions is 0.059. At the same time, under the same IM conditions, the mean DM values of the near-fault ground motions are greater than those of far-field ground motions. Therefore, under the same PGA conditions, near-fault pulsed ground motions have relatively stronger damage to tunnel structures than far-field ground motions.

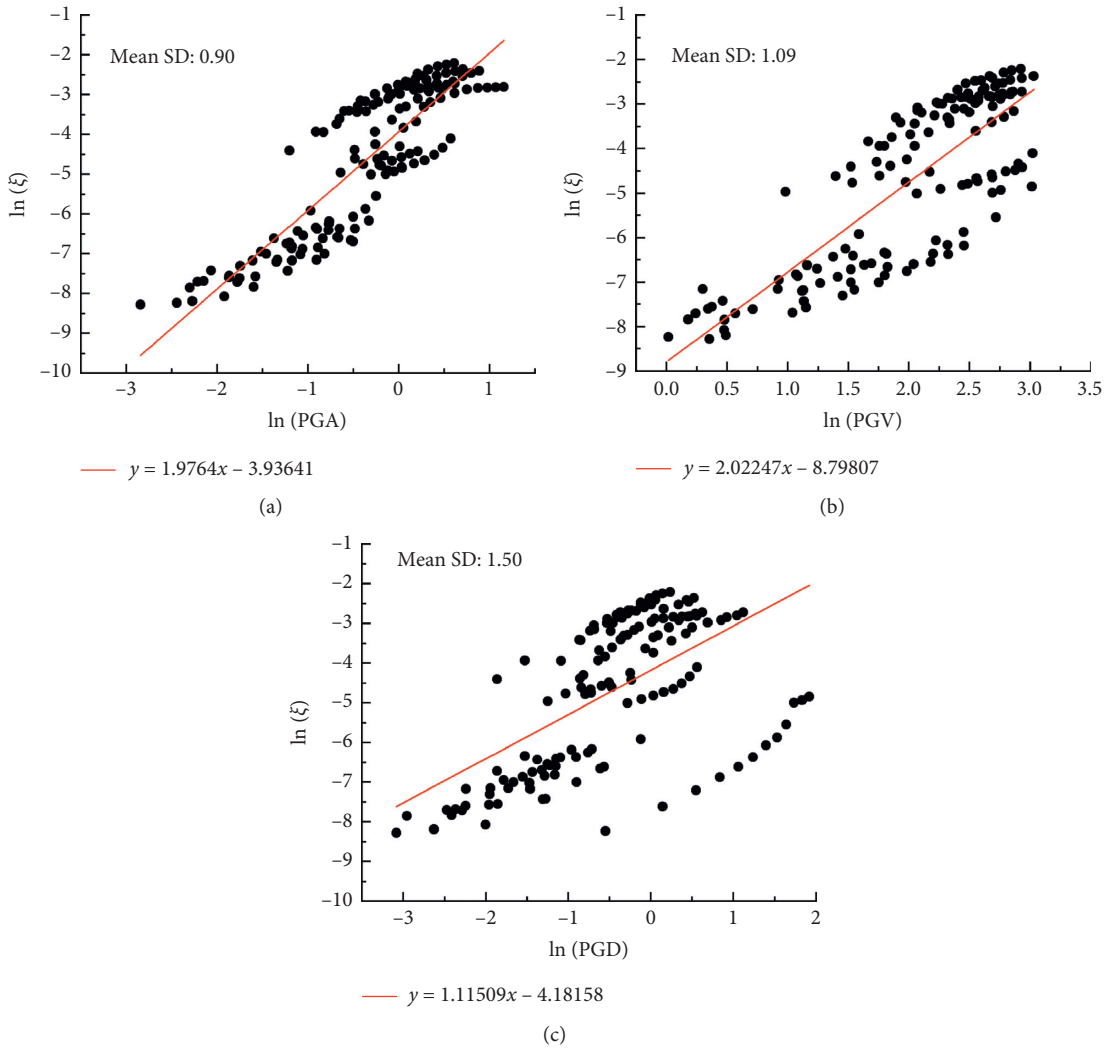

Figure 8: The regression fitting of different IM indicators: (a) PGA; (b) PGV; (c) PGD.

Table 5: Three-level fortification requirements and its control index thresholds.

Fortification requirement	Fortification target	Performance level	Threshold
I	After the earthquake, the tunnel is not damaged or slightly damaged and can maintain its normal service function	Normal service	$\xi_1 = 0.6\%$
II	The tunnel may be damaged after the earthquake. After repairing, its normal service function can be restored in a short time	Available after repairing	$\xi_2 = 2.5\%$
III	After the earthquake, the tunnel may occur major damage but does not collapse and can be opened to traffic at a speed limit after emergency repairing	Life threatened	$\xi_3 = 4\%$

Table 6: Seismic failure grades of tunnel structure based on relative deformation ratio.

Damage level	Intact	Slightly damaged	Moderately damaged	Severely damaged
Relative deformation ratio ξ	<0.6%	0.6% ~ 2.5%	2.5%~4%	>4%

Fit each IDA curve separately to obtain the IM value corresponding to the structural damage performance index threshold under the three-level support requirement. It is assumed that these IM values obey the lognormal distribution [45]. And then, the mean and standard deviation of the logarithmic values of these IM values are obtained, so that the probability distribution functions under the support requirements at all levels are

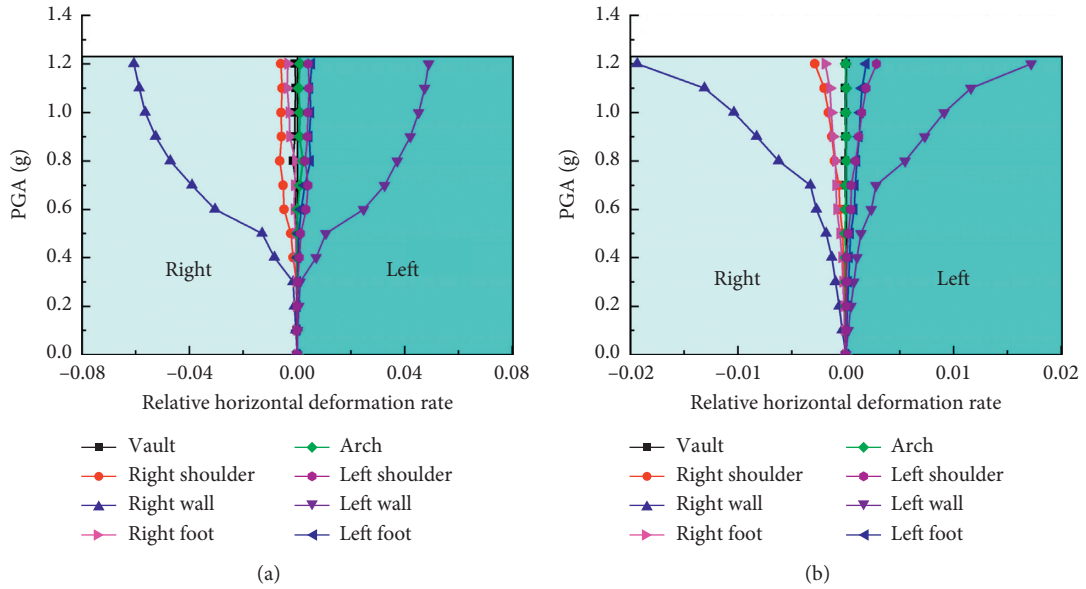

Figure 9: The vulnerable area of different characteristic locations of the tunnel section under action of different ground motions: (a) near-fault pulsed; (b) far-field.

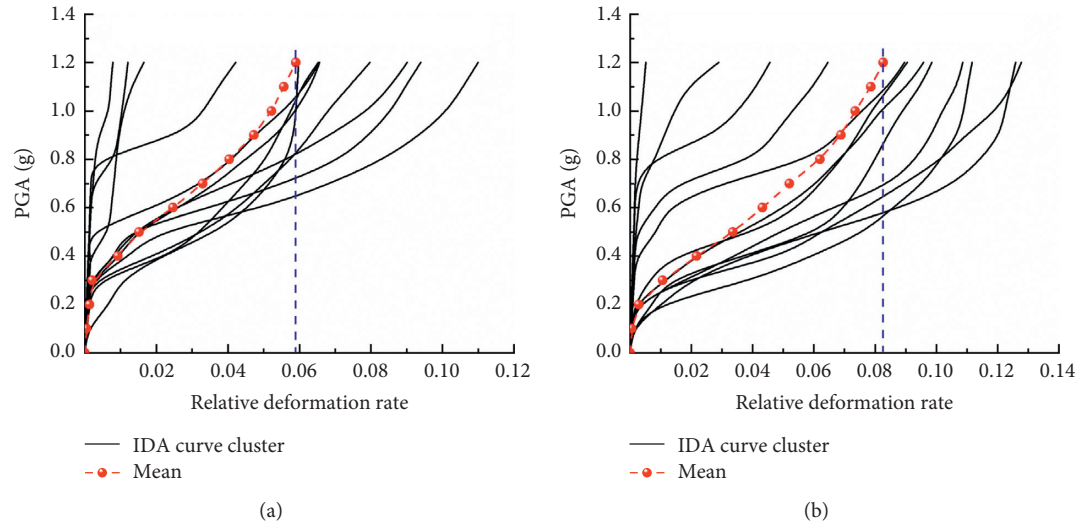

Figure 10: The IDA curve clusters under the action of different ground motions: (a) near-fault pulsed; (b) far-field.

calculated and the corresponding probability values are found. Finally, the seismic vulnerability curve can be drawn by taking the probability value as the ordinate and the corresponding IM value as the abscissa, as shown in Figure 11.

The same trend of the seismic vulnerability curve of the tunnel structure is observed under the action of these different ground motions because it is assumed that these IM values obey the lognormal distribution. Meanwhile, there is only a certain difference in the probability value, indicating that the destructive capacity of these two kinds of ground motions on the tunnel structure has a certain difference. Then, the probabilities of exceeding each seismic performance level under the action of different ground motions are obtained, as given in Table 7.

Take the highest probability of earthquake occurrence (the VIII frequent ground motion exceeding 63% in 50 years) and the highest earthquake intensity (the VIII extremely rare ground motion exceeding 1% in 100 years) as examples, respectively. Under the action of the near-fault pulsed ground motions at the level of VIII frequent, the probability of the tunnel structural damage exceeding the level of normal service is 55.01%, the probability of exceeding the level of available after repairing is 9.12%, and the probability of exceeding the level of life threatened is 5.59%. However, under the same level of far-field ground motions,

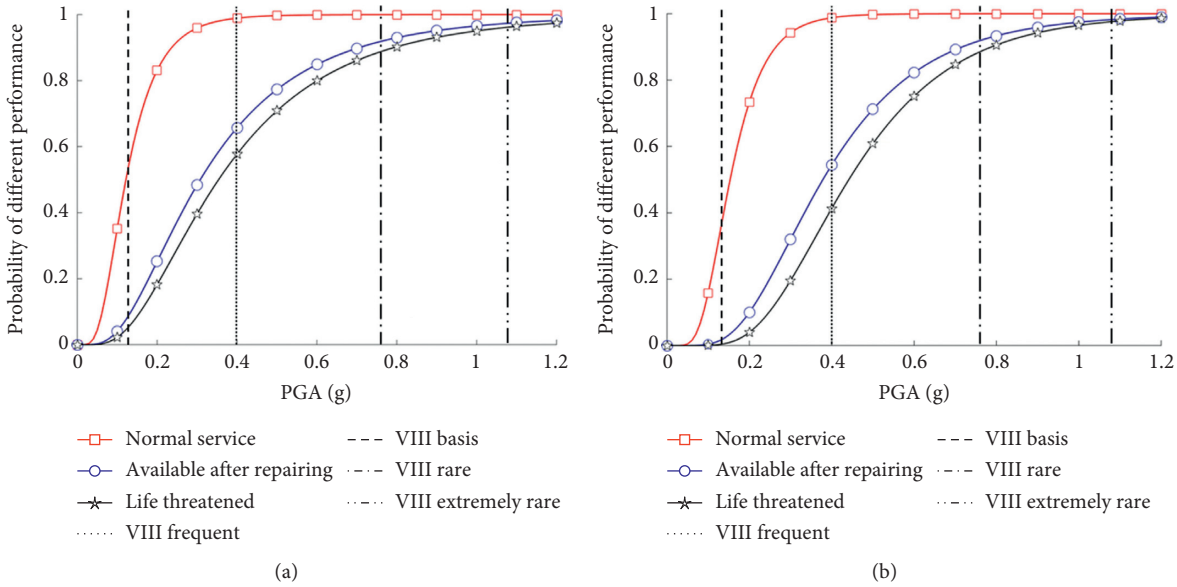

Figure 11: The seismic vulnerability curve of the tunnel structure under the action of different ground motions: (a) near-fault pulsed; (b) far-field.

Table 7: Exceeding probabilities under fortification standards responding to different ground motions.

Ground motions	Fortification standards	Normal service	Exceed probability/% available after repairing	Life threatened
Near-fault pulsed ground motions	VIII frequent	55.01	9.12	5.59
	VIII basis	98.93	65.68	57.70
	VIII rare	99.98	91.87	88.77
	VIII extremely rare	100.00	98.24	97.62
Far-field ground motions	VIII frequent	34.96	1.60	0.34
	VIII basis	98.79	54.39	41.32
	VIII rare	99.99	91.91	88.54
	VIII extremely rare	100.00	97.38	96.19

Table 8: Failure probabilities under fortification standards responding to different ground motions.

Ground motions	Fortification standards	Failure probability (%)			
		Intact	Slightly damaged	Moderately damaged	Severely damaged
Near-fault pulsed ground motions	VIII frequent	44.99	45.89	3.53	5.59
	VIII basis	1.07	33.25	7.98	57.70
	VIII rare	0.02	8.11	3.10	88.77
	VIII extremely rare	0.00	1.76	0.62	97.62
Far-field ground motions	VIII frequent	65.04	33.36	1.26	0.34
	VIII basis	1.21	44.40	13.07	41.32
	VIII rare	0.01	8.08	3.37	88.54
	VIII extremely rare	0.00	2.62	1.19	96.19

the probability of the tunnel structural damage exceeding the level of normal service is 34.96%, the probability of exceeding the level of available after repairing is 1.60%, and the probability of exceeding the level of life threatened is only 0.34%. Under the action of the near-fault pulsed ground motions and far-field ground motions at the level of VIII extremely rare, the probabilities of tunnel structural damage exceeding the level of normal service both are 100%. As for the probability of exceeding the level of life threatened and available after repairing, the ground motions of near-fault pulsed are larger than the far-field ground motions, of which 98.24% and 97.62% are under the near-fault pulsed ground

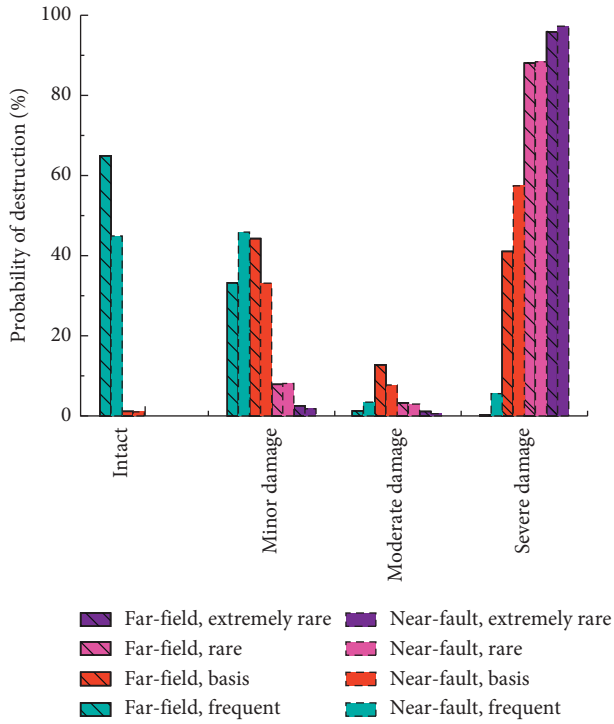

Figure 12: The failure probability of the tunnel structure under the action of different ground motions: (a) near-fault pulsed; (b) far-field.

motions, while 97.38% and 96.19% are under the far-field ground motions.

5. Discussion

Combined with the classification of the seismic performance level in Table 6, the failure probabilities of these two kinds of ground motions causing different degrees of damage to the tunnel structure under the action of earthquakes with different exceed probabilities is given in Table 8. Under the action of far-field ground motions at the level of frequent earthquakes, the probability that the tunnel structure is slightly damaged or even remains intact is 98.40%, while the probability of the same level of structural damage under the near-fault pulsed ground motions is only 90.88%. Under the action of near-fault pulsed ground motions at the extremely rare level, the probability of severely damaged to the tunnel structure is 97.62%, which is greater than the probability under the action of the same intensity of far-field ground motions that is 96.19%. Figure 12 shows the probability of different degrees of damage to the tunnel structure. At the same time, the trend in the probability of severely damaged on the tunnel structure under the action of earthquakes with different exceeding probability is observed, as shown in Figure 13. With the intensity of the ground motions increases, the tunnel structure is more likely to suffer more serious damage. Meanwhile, under the action of ground motions with the same support level, the near-fault pulsed ground motions are more likely to cause more serious

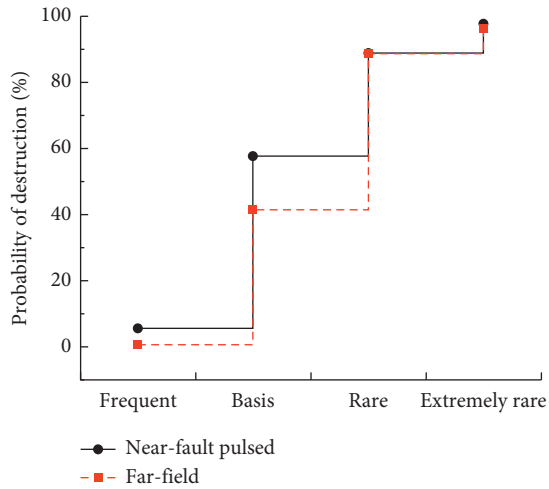

Figure 13: The destruction probability of the tunnel structure under the action of different ground motions: (a) near-fault pulsed; (b) far-field.

damage to the tunnel structure. That is to say, compared with the far-field ground motions, the near-fault pulsed ground motions have a stronger destructive ability on the tunnel structure, which could be attributed to the more powerful energy provided by the velocity pulses of near-fault pulsed ground motions. This statement is consistent with the opinion of Somerville [46].

6. Conclusions

In this study, the effects of velocity pulses on the seismic response and seismic performance of the tunnel structure are determined. The IDA method is introduced to the research field of seismic performance on railway tunnel engineering. The following conclusions are drawn:

(1) A recently developed velocity pulse equivalent model is proposed to synthesize the artificial near-fault pulsed ground motion, which is combined with the specific site attenuation characteristics of ground motions.

(2) The three-level support performance requirements suitable to railway tunnels are divided, and the PGA for the different intensity earthquakes is determined. Through regression fitting of different IM indicators and corresponding results, the effect of different IM indicators on the dispersion of IDA results is discussed, so that PGA is selected as the IM indicator.

(3) The near-fault pulsed ground motion is more destructive to the tunnel structure than the far-field ground motion under the same earthquake intensity, which is associated with the energy provided by the velocity pulse. Meanwhile, under the action of ground motions with the same support level, the near-fault pulsed ground motion is more likely to cause more serious damage to the tunnel structure. Therefore, in the seismic design of tunnel engineering, the impact of the velocity pulse effect of near-fault pulsed ground motion on the seismic performance of tunnel structures cannot be ignored.

(4) The lining deformation on the sidewalls on both sides of the tunnel is the most serious, which is the vulnerable area under a ground motion excitation and can be regarded as a weak part of the tunnel structure for the seismic design.

(5) In current manuscript, the influence of the quantity of ground motions to the selection of the IM is neglected in IDA analysis, which will be noted in the future work. In additional, the concrete damage model will be considered for the lining that will lead to some more interesting conclusions.

Abbreviations

c: Cohesion
C_s: The wave velocity
DGML: Design Ground Motion Library
DM: Damage measure
E: Young's modulus
f: The frequency of input motions
f_t: Normal tensile strength of the interface
G_s: The shear modulus of the field
IDA: Incremental dynamic analysis
IM: Intensity measure
l: The linear distance between the left foot and the right shoulder
M_w: The moment magnitude of earthquake
n: The number of calculation for nonlinear dynamic time history analysis
PBEE: Performance-based earthquake engineering
PEER: Pacific Earthquake Engineer Research Center Database
PGA: Peak value of acceleration of ground motion
PGD: Peak value of displacement of ground motion
PGV: Peak value of velocity of ground motion
Ratio: The larger value of the ratio of the positive and negative velocity peaks
S: The average standard deviation
$S_a(T_1, 5\%)$: The response spectrum of acceleration
t_0: The start time of velocity pulse
T: The seismic period
T_g: The characteristic period of the response spectrum
T_p: The pulse period
V_p: The peak pulse velocity
V_{p1}: The positive velocity peak of ground motion
V_{p2}: The negative velocity peak of ground motion
ν: Poisson's ratio
β: Dynamic amplification factor
ρ: Density
$\varnothing$: Friction angle
Δh_1: Horizontal displacement of the left foot
Δh_2: Vertical displacement of the left foot
Δl: The maximum grid size
Δv_1: Horizontal displacement of the right shoulder
Δv_2: Vertical displacement of the right shoulder
ξ: Relative deformation rate
λ: Wavelength corresponding to the maximum frequency.

Data Availability

The data used to support the findings of this study are included within the article.

Conflicts of Interest

The authors declare that they have no conflicts of interest.

Acknowledgments

The study was financially supported by the National Natural Science Foundation of China (51779253 and 52079133) and the National Basic Research Program of China (2015CB057905). The authors want to thank all the members who give them lots of help and cooperation.

References

[1] Y. Ates, D. Bruneau, and W. R. Ridgway, *An evaluation of potential effects of seismic events on a used fuel disposal fault*, AECL, Chalk River, Canada, 1995.

[2] N. Barton, "Effect of rock mass deformation on tunnel performance in seismic regions," *Advances in Tunnelling Technology and Subsurface Use*, vol. 4, pp. 89–99, 1984.

[3] D. Ma, H. Y. Duan, J. F. Liu, X. B. Li, and Z. L. Zhou, "The role of gangue on the mitigation of mining-induced hazards and environmental pollution: an experimental investigation," *Science of the Total Environment*, vol. 664, pp. 436–448, 2019.

[4] M. A. Hashash Youssef, J. Hook Jeffrey, B. Schmidt, and J. I. C. Yao, "Seismic design and analysis of underground structures," *Tunnelling and Underground Space Technology*, vol. 16, no. 4, pp. 247–293, 2001.

[5] Z. Z. Wang and Z. Zhang, "Seismic damage classification and risk assessment of mountain tunnels with a validation for the 2008 Wenchuan earthquake," *Soil Dynamics and Earthquake Engineering*, vol. 45, pp. 45–55, 2013.

[6] E. B. Aygar and C. Gokceoglu, "Problems encountered during a railway tunnel excavation in squeezing and swelling materials and possible engineering measures: a case study from Turkey," *Sustainability*, vol. 12, no. 3, Article ID 1166, 2020.

[7] Z. Chen, C. Shi, and T. Li, "Damage characteristics and influence factors of mountain tunnels under strong earthquakes," *Natural Hazards*, vol. 61, no. 2, pp. 387–401, 2012.

[8] S. Hashimoto, Y. Fujino, and M. Abe, "Damage analysis of hanshin expressway viaducts during 1995 kobe earthquake. II: damage mode of single reinforced concrete piers," *Journal of Bridge Engineering*, vol. 10, no. 1, pp. 54–60, 2005.

[9] Z. Z. Wang, B. Gao, Y. J. Jiang et al., "Investigation and assessment on mountain tunnels and geotechnical damage after the Wenchuan earthquake," *Science in China (Series E: Technological Sciences)*, vol. 52, no. 2, pp. 546–558, 2009.

[10] E. B. Aygar and C. Gokceoglu, "A special support design for a large-span tunnel crossing an active fault (T9 tunnel, ankara-sivas high-speed railway project, Turkey)," *Environmental Earth Sciences*, vol. 80, no. 1, p. 37, 2021.

[11] H. Yan, J. Zhang, B. Li, and C. Zhu, "Crack propagation patterns and factors controlling complex crack network formation in coal bodies during tri-axial supercritical carbon dioxide fracturing," *Fuel*, vol. 286, Article ID 119381, 2021.

[12] S. Li and L. Xie, "Progress and trend on near-field problems in civil engineering," *Acta Seismologica Sinica*, vol. 20, no. 1, pp. 102–111, 2007.

[13] J. Zhang and Y. Wang, "An ensemble method to improve prediction of earthquake-induced soil liquefaction: a multi-dataset study," *Neural Computing and Applications*, vol. 33, no. 2, pp. 1533–1546, 2020.

[14] M. Shimizu, T. Suzuki, S. Kato, Y. Kojima, K. Yashiro, and T. Asakura, "Historical damage of tunnels in japan and case studies of damaged railway tunnels in the mid niigata prefecture earthquakes," in *Proceedings of the the 33rd ITA-AITES World Tunnel Congress*, Prague, Czech Republic, May 2007.

[15] G. W. Housner and D. E. Hudson, "The port Hueneme earthquake of March 18, 1957," *Bulletin of The Seismological Society of America*, vol. 48, no. 2, pp. 163–168, 1958.

[16] Z. Cui, S. Qian, L. Xianlun et al., "Effects of near-fault ground motion on seismic response of underground caverns," *Rock and Soil Mechanics*, vol. 34, no. 11, pp. 3213–3222, 2013.

[17] Z. Cui and S. Qian, "Seismic response of underground rock cavern dominated by a large geological discontinuity subjected to near-fault and far-field ground motions," *Chinese Journal of Rock Mechanics and Engineering*, vol. 36, no. 1, pp. 53–67, 2017.

[18] J. Song and G. Gao, "Empirical predictive model for seismic displacement of slopes under velocity pulse-like ground motions," *Chinese Journal of Geotechnical Engineering*, vol. 35, no. 11, pp. 2009–2017, 2013.

[19] B. Todorov and A. H. M. M. Billah, "Seismic fragility and damage assessment of reinforced concrete bridge pier under long-duration, near-fault, and far-field ground motions," *Structures*, vol. 31, pp. 671–685, 2021.

[20] Ke Du, F. Cheng, J. Bai, and S. Jin, "Seismic performance quantification of buckling-restrained braced RC frame structures under near-fault ground motions," *Engineering Structures*, vol. 211, pp. 0141–0296, 2020.

[21] R. Sharbati, R. Rahimi, M. R. Koopialipoor et al., "Detection and extraction of velocity pulses of near-fault ground motions using asymmetric Gaussian chirplet model," *Soil Dynamics and Earthquake Engineering*, vol. 133, pp. 0267–7261, 2020.

[22] Federal Emergency Management Agency, *FEMA-445: Next-Generation Performance-Based Seismic Design Guideline*, Federal Emergency Management Agency, Washington, DC, USA, 2006.

[23] L. Xie, Y. Ma, and C. Zhai, *Performance-based Seismic Design and Design Ground Motion*, Science Press, Beijing, China, 2009.

[24] S. A. Argyroudis and K. D. Pitilakis, "Seismic fragility curves of shallow tunnels in alluvial deposits," *Soil Dynamics and Earthquake Engineering*, vol. 35, pp. 1–12, 2012.

[25] D. Vamvatsikos, *Seismic Performance Capacity and Reliability of Structures as Seen through Incremental Dynamic Analysis*, Stanford University, Stanford, CA, USA, 2002.

[26] D. Vamvatsikos and C. A. Cornell, "Incremental dynamic analysis," *Earthquake Engineering and Structural Dynamics*, vol. 31, no. 3, pp. 491–514, 2002.

[27] Z. Cui, S. Qian, L. Xianlun, and Z. Zhu, "Performance-based seismic stability assessment of large underground carven complex with incremental dynamic analysis," *Chinese Journal of Rock Mechanics and Engineering*, vol. 31, no. 4, pp. 703–712, 2012.

[28] Z. Zhong, Y. Shen, H. Yaru, L. Y. Li, and X. L. Du, "Seismic fragility analysis of two-story and three-span metro station structures based on IDA method," *Chinese Journal of Geotechnical Engineering*, vol. 42, no. 5, pp. 916–924, 2020.

[29] D. Ma, H. Y. Duan, Q. Zhang et al., "A numerical gas fracturing model of coupled thermal, flowing and mechanical effects," *Computers, Materials & Continua*, vol. 65, no. 3, pp. 2123–2141, 2020.

[30] D. Ma, J. X. Zhang, H. Y. Duan et al., "Reutilization of gangue wastes in underground backfilling mining: overburden aquifer protection," *Chemosphere*, vol. 264, no. 1, Article ID 128400, 2021.

[31] Y. Shen, Bo Gao, X. Yang, and S. Tao, "Seismic damage mechanism and dynamic deformation characteristic analysis of mountain tunnel after Wenchuan earthquake," *Engineering Geology*, vol. 180, pp. 85–98, 2014.

[32] The Professional Standards Compilation of People's Republic of China (Gb 50010-2010), *Code for Design of concrete Structures*, China Architecture &Building Press, Beijing, China, 2010.

[33] The Professional Standards Compilation of People's Republic of China (Gb/T 50218-2014), *Standard for Engineering Classification of Rock Mass*, China Planning Press, Beijing, China, 2014.

[34] D. Ma, H. Y. Duan, X. B. Li, Z. H. Li, Z. L. Zhou, and T. B. Li, "Effects of seepage-induced erosion on nonlinear hydraulic properties of broken red sandstones," *Tunnelling and Underground Space Technology*, vol. 91, Article ID 102993, 2019.

[35] H. Yan, J. Zhang, N. Zhou, and L. Meng, "Application of hybrid artificial intelligence model to predict coal strength alteration during CO_2 geological sequestration in coal seams,"

Science of the Total Environment, vol. 711, Article ID 135029, 2020.

[36] J. Zhang, F. Jiang, J. Yang et al., "Rockburst mechanism in soft coal seam within deep coal mines," *International Journal of Mining Science and Technology*, vol. 27, no. 3, pp. 551–556, 2017.

[37] L. Ming, *Study of the Effect of Near-Fault Ground Motion on Structural Seismic Design*, Harbin: Institute of engineering mechanics, China earthquake administration, Harbin, China, 2010.

[38] S. Huang, *Research on Failure Mechanism and Aseismic Measures for Underground Engineering under High Intensity Earthquake*, Wuhan institute of rock and soil mechanics, Chinese Academy of Sciences, Wuhan, China, 2010.

[39] Y. Tian, Q. Yang, and M. Lu, "Simulation method of near-fault pulse-type ground motion," *Acta Seismologica Sinica*, vol. 20, no. 1, pp. 77–84+114, 2007.

[40] The Professional Standards Compilation of People's Republic of China (Gb 18306-2015), *Seismic Ground Motion Parameters Zonation Map of China*, Standards Press of China, Beijing, China, 2015.

[41] B. Wang, X. Wang, L. Yang et al., "Seismic performance analysis of highway tunnel lining based on IDA," *Railway Standard Design*, vol. 64, no. 5, pp. 96–102, 2020.

[42] C. Xiang, *Study on Performance-Based Seismic Design Method for Highway Tunnel Structure*, Chongqing Jiaotong University, Chongqing, China, 2017.

[43] X. Lu, L. Ye, Z. Miao et al., "Elasto-plastic analysis of buildings against earthquake-theory," *Model and Implementation in ABAQUS, MSC.MARC and SAP2000*, pp. 112–124, China Architecture and Building Press, Beijing, China, 2009, in Chinese.

[44] The Professional Standards Compilation of People's Republic of China (Gb 50111-2006), *Code for Seismic Design of Railway Engineering*, Standards Press of China, Beijing, China, 2006.

[45] K. R. Karim and F. Yamazaki, "Effect of earthquake ground motions on fragility curves of highway bridge piers based on numerical simulation," *Earthquake Engineering and Structural Dynamics*, vol. 30, no. 12, pp. 1839–1586, 2001.

[46] P. Somerville, "Characterizing near fault ground motion for the design and evaluation of bridges," in *Proceedings of the 3rd National Seismic Conference and Workshop on Bridges and Highways*, pp. 137–148, State University of New York at Buffalo, Buffalo, New York, January 2002.